LETTERS

Transient nature of late Pleistocene climate variability

Thomas J. Crowley[1] & William T. Hyde[2]

Climate in the early Pleistocene[1] varied with a period of 41 kyr and was related to variations in Earth's obliquity. About 900 kyr ago, variability increased and oscillated primarily at a period of ~100 kyr, suggesting that the link was then with the eccentricity of Earth's orbit. This transition has often[2–5] been attributed to a non-linear response to small changes in external boundary conditions. Here we propose that increasing variablility within the past million years may indicate that the climate system was approaching a second climate bifurcation point, after which it would transition again to a new stable state characterized by permanent mid-latitude Northern Hemisphere glaciation. From this perspective the past million years can be viewed as a transient interval in the evolution of Earth's climate. We support our hypothesis using a coupled energy-balance/ice-sheet model, which furthermore predicts that the future transition would involve a large expansion of the Eurasian ice sheet. The process responsible for the abrupt change seems to be the albedo discontinuity at the snow–ice edge. The best-fit model run, which explains almost 60% of the variance in global ice volume[6] during the past 400 kyr, predicts a rapid transition in the geologically near future to the proposed glacial state. Should it be attained, this state would be more 'symmetric' than the present climate, with comparable areas of ice/sea-ice cover in each hemisphere, and would represent the culmination of 50 million years of evolution from bipolar nonglacial climates to bipolar glacial climates.

A recent composite[1] of benthic $\delta^{18}O_{cal}$ (that is, calcite) records summarizes the general pattern of climate back to 3.0 Myr ago (Fig. 1a). A 500-kyr moving boxcar window (see ref. 5) highlights long-term changes in $\delta^{18}O_{cal}$ variability (Fig. 1b). This window length was chosen to mute glacial–interglacial variations and any possible influence of the 413-kyr eccentricity cycle. There is an increase in variability after the Pliocene/Pleistocene boundary (~1.8 Myr ago), with clear evidence for steps ~665 kyr and ~885 kyr ago. The trend is similar (Fig. 1b) to strontium isotope changes[7] that are sometimes interpreted to reflect variations in continental weathering.

Histograms (Fig. 1c) of equal-sized, 450-kyr sections of the latest Pleistocene indicate continued evolution and bimodality, with an interglacial mode being more common in the earlier section. Despite the presence of more extreme interglacial states in the later section (Fig. 1a), its mean $\delta^{18}O_{cal}$ value is isotopically heavier (about 0.1‰, equivalent to ~10 m in sea-level change), and the glacial mode is more common. Two of the four most extreme $\delta^{18}O_{cal}$ maxima occurred during the last two glacial periods (Fig. 1a). The above changes, plus a smaller step ~1.12 Myr ago, correspond to Pleistocene 'megacycle' boundaries identified[8] in major European glacial advances and European and Chinese loess sequences.

Trends in variability may also apply on millennial scales. A core[9] from the subpolar North Atlantic (Fig. 1d) suggests generally enhanced variability from glacial stage 12 (~430 kyr ago) to stages 2–4 of the last glacial cycle. However, this interpretation requires further testing.

Because prior energy-balance modelling (EBM) work (see fig. 4 of ref. 10) suggests that enhanced variability may indicate a system near a climate bifurcation point, one interpretation of the observed Pleistocene trend is that the system was poised to flip to a different climate state. We test this hypothesis by employing, without significant modification, a published version of an energy-balance/ice-sheet model[11]. The coupled model consists of four submodels that predict ice flow, mass balance, temperature and bedrock sinking. Ice is assumed to flow subject to a temperature-independent rheology. Ice sheets are driven by a uniform precipitation of $0.6\,m\,yr^{-1}$ that decreases with height and temperature. This value is characteristic of current Northern Hemisphere mid-latitude land areas. Precipitation is computed according to statistical models, which themselves take as input monthly temperatures from a nonlinear, two-dimensional (latitude–longitude grid), diffusive seasonal EBM[12]. Bedrock sinking is assumed to occur with a time constant of 4 kyr. The ice-sheet model has a resolution of $0.5^\circ \times 0.5^\circ$. The time step for the EBM is 40 yr, whereas for the ice-sheet model it is never more than 20 yr and, during times of rapid change, is as small as 2.5 yr. The coupled model has been previously applied to topics ranging from millennial variability to Neoproterozoic glaciation[13,14].

The coupled model is forced with orbital insolation variations as derived in ref. 15. To isolate as much as possible the inherent response of the ice sheet, we do not consider glacial–interglacial changes in CO_2 or North Atlantic heat sources.

Plotting operating curves (Fig. 2a) is a standard method of depicting model behaviour, with solar constant changes used as a proxy for other changes in boundary conditions. As radiative forcing decreases, there is an approximately linear increase in ice volume until the model reaches a critical point. Over an interval of $1.4\,W\,m^{-2}$ (less than the ice age change in radiative forcing from CO_2), variability increases substantially. The solution then stabilizes on a second branch, after which ice volume again changes nearly linearly with forcing. Simulated ice sheets (Fig. 3a–c) indicate that the North American and Eurasian ice sheets are broadly similar in location to, but only about half the volume of, those observed for the last glacial maximum. Glacial–interglacial CO_2 variations are a plausible explanation for the principal difference, with the lack of a variable North Atlantic heat source perhaps contributing additionally to Eurasian ice-volume changes.

As suggested by theory, variability reaches a maximum in the transition zone (Fig. 2b) and is virtually the same for the two stable states, despite their having very different ice-volume levels. In the middle of the rapid growth phase of the North American ice sheet, a very large Eurasian ice sheet (Fig. 2a) develops from a perturbation of only $0.07\,W\,m^{-2}$ (three times smaller than the radiative forcing from the 11-yr solar cycle). This ice sheet (Fig. 3d) is more than twice the

[1]School of Geosciences, The University of Edinburgh, Edinburgh EH9 3JW, UK. [2]Department of Physics, The University of Toronto, Toronto, Ontario M5S 1A7, Canada.

©2008 Macmillan Publishers Limited. All rights reserved

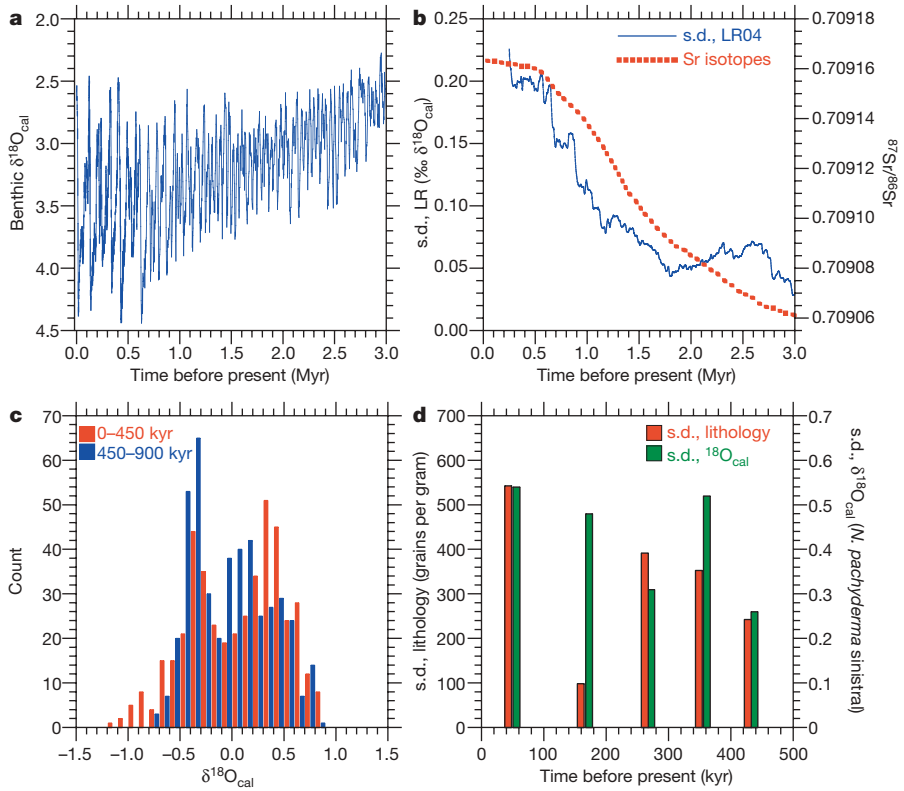

Figure 1 | Evidence for trends in climate variability in the Plio-Pleistocene. **a**, Plio-Pleistocene composite $\delta^{18}O_{cal}$ record from ref. 1; more positive values indicate colder climates. ($\delta^{18}O = (^{18}O/^{16}O)_{sample}/(^{18}O/^{16}O)_{standard} - 1$ is a measure of the difference in a sample, with respect to a standard, in the stable isotope ratios of ^{18}O to ^{16}O, usually expressed in parts per thousand.) **b**, 500-kyr moving-boxcar-windowed standard deviation of the record in **a** (termed LR in label) compared with the $^{87}Sr/^{86}Sr$ isotope record from ref. 7; the trend in $\delta^{18}O_{cal}$ variability is relatively robust to changes in window width. **c**, Histograms of $\delta^{18}O_{cal}$ composite (with mean removed) for the past 900 kyr (see text), divided into two equal subsamples; more negative values are interpreted as having less ice volume. **d**, Standard deviations of two indices of variability within the five glacial stages of the last 0.5 Myr in densely sampled parts of a subpolar North Atlantic core[9], showing a general increase in within-stage variations (towards the present) of lithic (ice-rafted) grains and the $\delta^{18}O_{cal}$ of cold-water planktonic foraminifer *Neogloboquadrina pachyderma* sinistral (left-coiling). This general 'increase towards the present' is similar to that found in orbital-scale variations (see text).

volume of the modelled North American ice sheet. Because our ice-sheet model does not allow for multi-doming, we probably overestimate[16] its volume by ~20%. Nevertheless, the general success of model simulations for the Pleistocene suggests that the prediction of a very large Eurasian ice sheet is not implausible; such a response has already been found in another model[17].

To determine whether patterns in the operating curves are within the range of inferred Plio-Pleistocene changes, we simulate the last 3.0 Myr using only orbital forcing plus long-term CO_2 changes. Although the strontium isotope curve (Fig. 1b) suggests a sigmoidal variation in weathering (and perhaps CO_2) since 3.0 Myr ago, for the sake of simplicity we mainly use linear ramp forcing (Fig. 4a; in one run, CO_2 stabilized at 240 p.p.m. 1.0 Myr ago). The initial Pliocene CO_2 level is constrained by leaf stomata data[18] at about 360 p.p.m., and the level at 0 Myr is set at the mean CO_2 level of the last 20 kyr (~240 p.p.m.). Because the original CO_2 reference level of the coupled ice-sheet model was 360 p.p.m., we adjust the outgoing radiative forcing term in the energy balance model to account for the anthropogenic effect. As the model may have some biases, relative changes in radiative forcing are probably a more reliable indicator of model behaviour than the absolute value of CO_2 at any particular time.

There are a number of interesting features of the model response to one small (~1.0–2.0 W m^{-2}), linear change in boundary conditions (Fig. 4). All runs extended beyond the present day (Fig. 4b) transition to the postulated second equilibrium climate state within a strikingly narrow mean CO_2 value of about 240 ± 5 p.p.m. The run with the smallest change (295–240 p.p.m.) has the highest correlation ($r = 0.70$) with the Plio-Pleistocene composite of ref. 1 (see Fig. 1a). Separation of the Northern Hemisphere trend into individual ice-sheet responses (Fig. 4c) indicates that, as in the operating curves, the North American ice sheet first crossed the bifurcation threshold

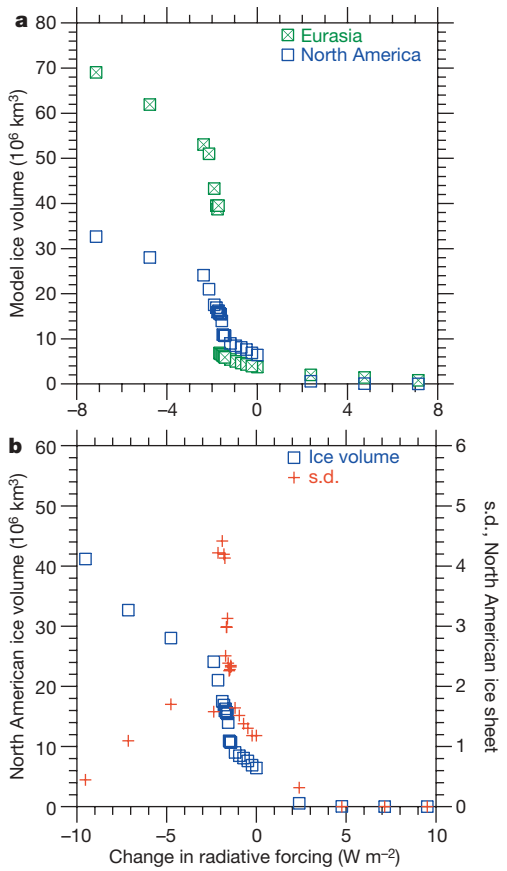

Figure 2 | Operating curves for climate/ice-sheet model as a function of the solar constant (abscissa). The standard value of the solar constant for the present is 1.0 (average for Earth, ~340 W m^{-2}). These units can be translated into equivalent CO_2 changes: a 1.5% change in the solar constant is approximately equivalent to a doubling of CO_2 (~3.7 W m^{-2}), after factoring in the 30% albedo of the Earth. **a**, Ice-volume changes for North America and Eurasia; (b) North American ice volume versus standard deviation for the 150–200-kyr interval of each of 36 model runs. Note that variability increases sharply near the bifurcation.

©2008 Macmillan Publishers Limited. All rights reserved

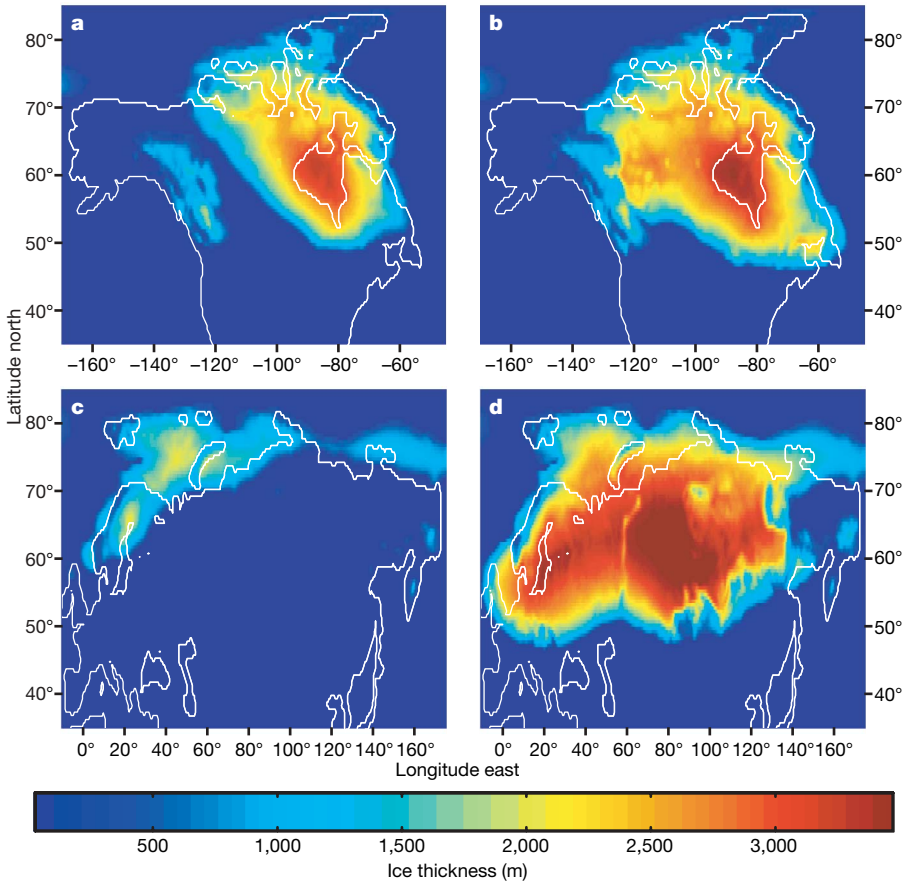

Figure 3 | Simulated ice extent for different stages of North American and Eurasian ice-sheet growth. **a**, Small North American ice sheet; **b**, large North American ice sheet; **c**, small Eurasian ice sheet; **d**, large Eurasian ice sheet that is the postulated second stable state for Northern Hemisphere glaciation.

~1.14 Myr ago, during a low-eccentricity interval. This coincides almost exactly with the beginning of one of the small steps (see above) in the variability curve (Fig. 1b). These responses are consistent with one explanation[12] for glacial inception: because North America is smaller than Eurasia, it will not warm up in the summer as much as Eurasia and, therefore, will respond earlier than Eurasia at a glaciation threshold.

In the last 0.6–0.7 Myr (Fig. 5a) of the best-fit run, lower frequency oscillations occur with ~100-kyr periods (as in observations). Although low-frequency oscillations are present in other runs, the flatter CO_2 ramp for the 295–240-p.p.m. run allows more time for ~100-kyr variability before transitioning to the large Eurasian ice sheet. Deglaciations are similar to 'terminations' in the marine $\delta^{18}O_{cal}$ record. In our model, rapid melting can be attributed to continued southward flow of the ice sheet into the isostatic depression it created[19]. An initial attempt to superimpose observed CO_2 changes[20] during the last 650 kyr triggered the Eurasian ice-sheet instability, most probably because of the model constraints addressed above.

There is agreement in both the time ($r = 0.77$) and the frequency domains (Fig. 5) of the scaled best-fit run with the $\delta^{18}O_{sw}$ best-guess[6] seawater reconstruction of global ice volume, with both records having substantially less ~100-kyr-ago power than the $\delta^{18}O_{cal}$ record (Fig. 5b). This difference reflects the deep-water temperature overprint on observed $\delta^{18}O_{sw}$. Model variability in the last 410 kyr is about 25% greater than in the preceding segment (Fig. 5a) and is primarily manifested in the ~23-kyr precession and 41-kyr obliquity bands (Fig. 5b). Model ~100-kyr-ago power is greater than a 'background' level from earlier in the record and is most strongly present in the North American ice sheet (Supplementary Fig. 1), first emerging in the 820–410-kyr segment and then increasing in the Eurasian ice sheet over the last 410-kyr segment. Again, it is necessary to recall that some frequency-domain differences between model and observations may be partly due to lack of glacial–interglacial CO_2 fluctuations in our runs, plus no attempt to simulate variable North Atlantic heat sources. Regardless, our results clearly indicate that ~100-kyr-ago power is embedded in the physics of the coupled climate/ice-sheet system and is not just a consequence of, for example, glacial–interglacial CO_2 variations[6].

For the best-fit run, transition to the large Eurasian ice sheet occurs shortly after the present (Fig. 5a). Our results therefore suggest that the actual climate system may have been geologically close (10^4–10^5 yr) to the final phase of a 50-Myr evolution from bipolar warm climates to permanent bipolar glaciation. (Presumably, future society could prevent this transition indefinitely with very modest adjustments to the atmospheric CO_2 level.)

Because our model has no ocean dynamics, rapid change requires a different explanation than the oft-discussed thermohaline instability. In our simulations, the instability resembles the well-known[21] albedo discontinuity at the snow–ice boundary. To persist, an ice cap must be stable against warming. This stability is conferred by the balance between the energy sink provided by the ice cap and the energy source (transport) onto the ice cap from warmer regions. The energy sink is a function of the ice cap's higher albedo (ameliorated by reduced infrared output from the higher, colder surface) and the size of the ice cap.

For radiative adjustment and transport values typical of the Earth, it has been analytically determined[22] that at a bifurcation point snow cover expands on a scale of ~1500–2000 km. This length scale can be found in mid/high-latitude instrumental records[23], some modelling studies[24–26] and the latitudinal shift associated with the large Eurasian ice sheet (see Fig. 3c, d). Our model also displays hysteresis behaviour characteristic of such systems[27].

©2008 Macmillan Publishers Limited. All rights reserved

In addition to the tests outlined in this paper, more complex ice-sheet models could be used. Even though these models are more 'realistic', we are not convinced that they would show a fundamentally different result. There is already a huge difference in complexity between the original EBM[21] and the model we use, yet to first order the bifurcation diagrams are the same. We hypothesize that the future behaviour of more complicated coupled models will be influenced as much by the albedo discontinuity as by any added features of ice-sheet complexity.

Observational tests involve the ~200 kyr before 400 kyr ago (Fig. 5a). If our agreement with the $\delta^{18}O_{sw}$ record is not a coincidence, then we predict that sea level/ice volume differences from present during the precession peaks ~480 and 500 kyr ago would be significantly less (on the order of 0 ± 10 m) than the ~20–25-m sea level drop suggested by the $\delta^{18}O_{cal}$ record (Fig. 1a). Because the $\delta^{18}O$ of atmospheric oxygen ($\delta^{18}O_{atm}$) is a good approximation to the $\delta^{18}O_{sw}$ estimate ($r = 0.92$), publication of the extended Dome C (Antarctica) $\delta^{18}O_{atm}$ record will be one test of our hypothesis.

Older geological intervals can also be used to test whether the entire transition to an alternative stable state may have occurred

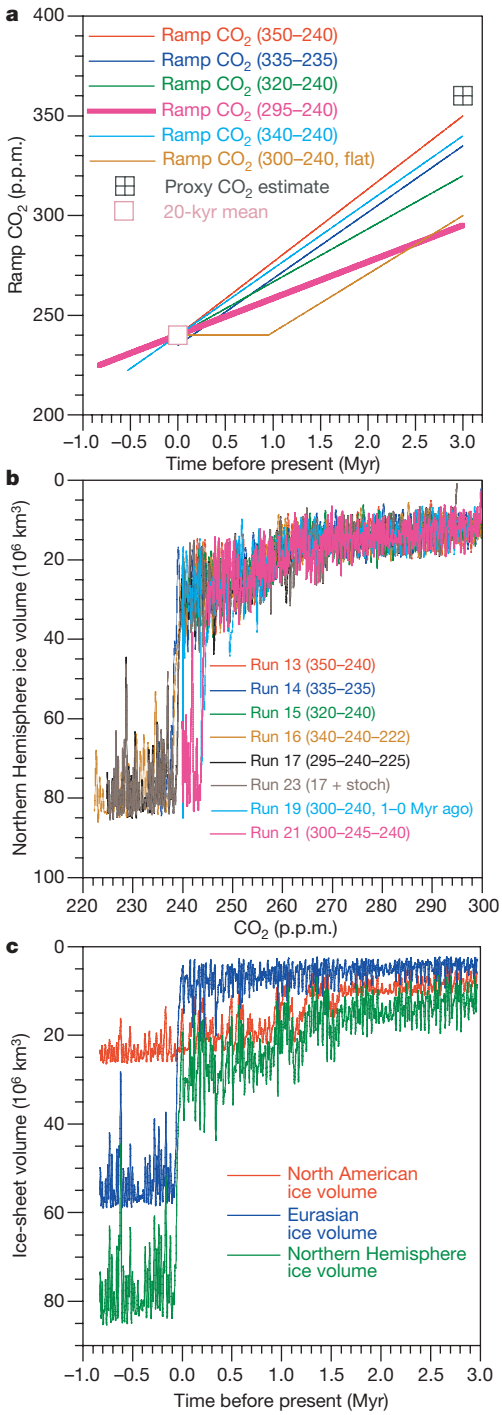

Figure 4 | Principal results of the ramp model runs. a, Plio-Pleistocene CO_2 scenarios for runs (see text); **b**, plots of Northern Hemisphere ice volume as a function of CO_2 for the different ramp scenarios. Labels refer to CO_2 values (p.p.m.) used for each run. In each label, the first value is the starting point, 3.0 Myr ago, and the second value is the end point, 0.0 Myr ago (except for run 19, in which the ramp stopped 1.0 Myr ago and constant CO_2 levels were used for the remaining 1.0 Myr). Where there is a third value, it refers to the future projection using the trend line for the corresponding run. In run 23, the best-fit run (run 17) was modified with a stochastic forcing of ~0.4 W m^{-2} to mimic decadal-scale oscillations. We note that, regardless of forcing scenario, runs generally transition to the large Eurasian ice sheet at a background CO_2 level of ~240 p.p.m. **c**, Details of the best-fit run (see Fig. 5) with respect to total ice volume and contribution from each ice sheet (see Supplementary Data).

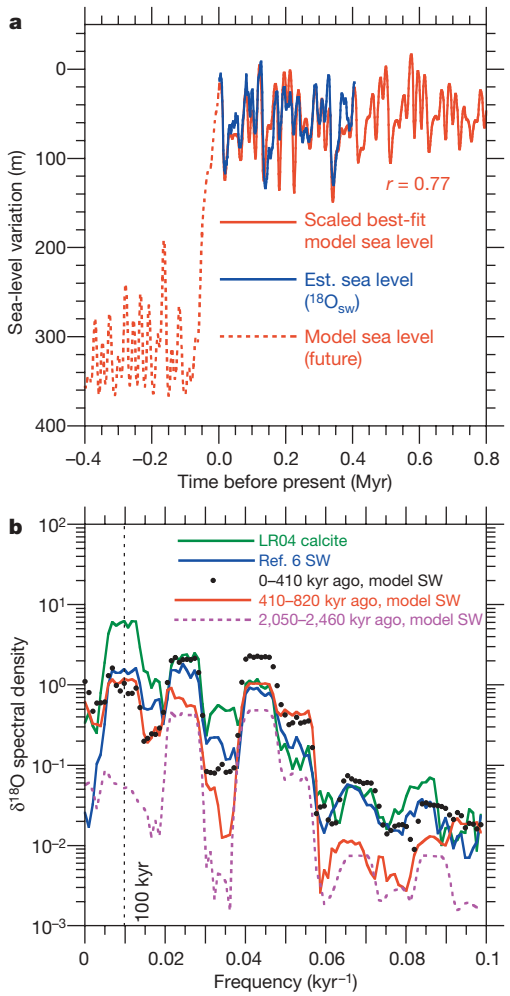

Figure 5 | Further analyses of best-fit run. a, Comparison with best-guess seawater ($\delta^{18}O_{sw}$) reconstruction of ref. 6, and projection into the future. **b**, Multi-taper-method frequency-domain comparison of the best-fit model with the results of ref. 6 and the $\delta^{18}O_{cal}$ records, and two earlier intervals of the best-fit model run. The ice-volume record for the best-fit run was converted to $\delta^{18}O_{sw}$ by setting the last interglacial best-guess value to −0.04‰ and matching the model to the preceding maximum in $\delta^{18}O_{sw}$ (see Supplementary Data). The mean value of the $\delta^{18}O_{sw}$ record of ref. 6 was also adjusted to set the last interglacial value to −0.04‰. All analyses were done for identical intervals of 410 kyr. Solid lines indicate a run was significant at the 95% level for 100-kyr-ago power (higher frequency intervals at 23 kyr and 41 kyr were always significant).

©2008 Macmillan Publishers Limited. All rights reserved

before. The advance of the Antarctic ice sheet to the edge of the continent near the Eocene/Oligocene boundary (~33.6 Myr ago) represents one possible case[28]. A composite benthic $\delta^{18}O_{cal}$ reconstruction[29] indicates that $\delta^{18}O_{cal}$ standard deviations of the ~400-kyr time intervals before and after the transition are nearly ~0.14‰, whereas during the transition (see Supplementary Fig. 2) the standard deviation is 80% higher (20% detrended). This response is consistent with our interpretation of multiple stable states. There were also numerous late Cenozoic oscillations of a wet-based East Antarctic ice sheet[30] before it transitioned to a cold-based glacier ~14 Myr ago, following which at least parts of it have apparently remained stable.

Finally, our hypothesis may be relevant to interpretation of millennial-scale variability in the late Pleistocene. The tentative link in Fig. 1b, d between orbital- and millennial-scale variability suggests that the many studies and interpretations of the latter may be missing a fundamental perspective, unless they are interpreted within the framework of the overall higher and (we suggest) transient variability on longer timescales.

Received 21 March; accepted 28 August 2008.

1. Lisiecki, L. E. & Raymo, M. E. A Pliocene-Pleistocene stack of 57 globally distributed benthic $\delta^{18}O$ records. *Paleoceanography* **20,** doi:10.1029/2004PA001071 (2005).
2. Maasch, K. & Saltzman, B. A low-order dynamical model of global climatic variability over the full Pleistocene. *J. Geophys. Res.* **95,** 1955–1963 (1990).
3. Berger, A., Li, X. S. & Loutre, M.-F. Modeling northern hemisphere ice volume over the last three million years. *Quat. Sci. Rev.* **18,** 1–11 (1999).
4. Huybers, P. Glacial variability over the last two million years: An extended depth-derived age model, continuous obliquity forcing, and the Pleistocene progression. *Quat. Sci. Rev.* **26,** 37–55 (2007).
5. Lisiecki, L. & Raymo, M. E. Plio-Pleistocene climate evolution: Trends and transitions in glacial cycle dynamics. *Quat. Sci. Rev.* **26,** 56–69 (2007).
6. Shackleton, N. J. The 100,000 year ice-age cycle identified and found to lag temperature, carbon dioxide, and orbital eccentricity. *Science* **289,** 1897–1902 (2000).
7. McArthur, J. M., Howarth, R. J. & Bailey, T. R. Strontium isotope stratigraphy: LOWESS version 3: Best fit to the marine Sr-isotope curve for 0–509 Ma and accompanying look-up table for deriving numerical age. *J. Geol.* **109,** 155–170 (2001).
8. Kukla, G. & Cilek, V. Plio-Pleistocene megacycles: Record of climate and tectonics. *Palaeogeogr. Palaeoclimatol. Palaeoecol.* **120,** 171–194 (1996).
9. McManus, J. F., Oppo, D. W. & Cullen, J. L. A 0.5 million year record of millennial scale climate variability in the North Atlantic. *Science* **283,** 971–975 (1999).
10. Crowley, T. J. & North, G. R. Abrupt climate change and extinction events in Earth history. *Science* **240,** 996–1002 (1988).
11. Tarasov, L. & Peltier, W. R. Terminating the 100 kyr ice age cycle. *J. Geophys. Res.* **18,** 21665–21693 (1997).
12. North, G. R., Mengel, J. G. & Short, D. A. Simple energy balance model resolving the seasons and the continents: Application to the astronomical theory of glaciation. *J. Geophys. Res.* **88,** 6576–6586 (1983).
13. Hyde, W. T. & Crowley, T. J. Stochastic forcing of Pleistocene ice sheets: Implications for the origin of millennial-scale climate oscillations. *Paleoceanography* **17,** 10.1029/2001PA000669 (2002).
14. Hyde, W. T., Crowley, T. J., Baum, S. K. & Peltier, W. R. Neoproterozoic 'Snowball Earth' simulations with a coupled climate/ice sheet model. *Nature* **405,** 425–429 (2000).
15. Berger, A. Long term variations of daily insolation and Quaternary climate changes. *J. Atmos. Sci.* **35,** 2362–2367 (1978).
16. Crowley, T. J. & Baum, S. K. Estimating Carboniferous sea-level fluctuations from Gondwanan ice extent. *Geology* **19,** 975–977 (1991).
17. Calov, R. & Ganopolski, A. Multistability and hysteresis in the climate-cryosphere system under orbital forcing. *Geophys. Res. Lett.* **32,** doi:10.1029/2005GL024518 (2005).
18. van der Burgh, J., Visscher, H., Dilcher, D. L. & Kurschner, W. M. Paleoatmospheric signatures in Neogene fossil leaves. *Science* **260,** 1788–1790 (1993).
19. Hyde, W. T. & Peltier, W. R. Sensitivity experiments with a model of the ice age cycle: The response to harmonic forcing. *J. Atmos. Sci.* **42,** 2170–2188 (1985).
20. Lüthi, D. *et al.* High-resolution carbon dioxide concentration record 650,000–800,000 years before present. *Nature* **453,** 379–382 (2008).
21. Budyko, M. I. The effect of solar radiation changes on the climate of the Earth. *Tellus* **21,** 611–619 (1969).
22. North, G. R. The small ice cap instability in diffusive climate models. *J. Atmos. Sci.* **41,** 3390–3395 (1984).
23. Hansen, J. E. & Lebedeff, S. Global trends of measured surface air temperature. *J. Geophys. Res.* **92,** 13345–13372 (1987).
24. Manabe, S. & Broccoli, A. J. The influence of continental ice sheets on the climate of an ice age. *J. Geophys. Res.* **90,** 2167–2190 (1985).
25. Crowley, T. J., Yip, K.-Y. J. & Baum, S. K. Snowline instability in a general circulation model: Application to Carboniferous glaciation. *Clim. Dyn.* **10,** 363–374 (1994).
26. Baum, S. K. & Crowley, T. J. The snow/ice instability as a mechanism for rapid climate change: A Neoproterozoic Snowball Earth model example. *Geophys. Res. Lett.* **30,** doi:10.1029/2003GL017333 (2003).
27. Crowley, T. J., Hyde, W. T. & Baum, S. K. CO_2 levels required for deglaciation of a "Near-Snowball" Earth. *Geophys. Res. Lett.* **28,** 283–286 (2001).
28. DeConto, R. M. & Pollard, D. Rapid Cenozoic glaciation of Antarctica induced by declining atmospheric CO_2. *Nature* **421,** 245–249 (2003).
29. Zachos, J., Pagani, M., Sloan, L., Thomas, E. & Billups, K. Trends, rhythms, and aberrations in global climate, 65 Ma to Present. *Science* **292,** 686–693 (2001).
30. Jamieson, S. S. R. & Sugden, D. E. in *Antarctica: A Keystone in a Changing World* (eds Cooper, A. K. & Raymond, C.) 39–54 (Proc. 10th Intl Symp. Antarctic Earth Sci., National Academies, 2008).

Supplementary Information is linked to the online version of the paper at www.nature.com/nature.

Acknowledgements This research received partial support the Scottish Alliance for Geoscience, the Environment, and Society (SAGES) and from the US National Science Foundation. We thank G. North for numerous discussions over the years and S. Obrochta for valuable assistance.

Author Contributions W.T.H. had primary responsibility for model simulations and T.J.C. for analysis of model output, comparison with geological data and write-up of results.

Author Information Reprints and permissions information is available at www.nature.com/reprints. Correspondence and requests for materials should be addressed to T.J.C. (thomas.crowley@ed.ac.uk).

©2008 Macmillan Publishers Limited. All rights reserved